# Pulmonary lobar segmentation from computed tomography scans based on statistical shape model

Zhang, Y.[1], Osanlouy, M.[1], Clark, A.R.[1], Hoffman, E.A.[2], Tawhai, M.H[1]

[1]Auckland Bioengineering Institute, University of Auckland, Auckland, NZ, [2]Department of Radiology and Biomedical Engineering, University of Iowa Carver College of Medicine, Iowa City, IA, US.

## Abstract

Automatic identification of lobes from imaging is important in lung disease assessment and treatment planning. In this study, we use a statistical shape model to guide lobar segmentation. By deforming an average lobar model onto an individual's lung shape, we predict fissure locations approximately, to refine our search region for lobar structures. Then, we use an eigenvalue of Hessian matrix analysis and a connected component eigenvector based analysis to determine a set of fissure-like candidate points. A smooth multi-level B-spline curve is fitted to the most fissure-like points (those with high fissure probability) and the fitted fissure plane is extrapolated to the lung boundaries. The method was tested on 20 inspiratory and expiratory CT scans in healthy young subjects and older subjects with idiopathic pulmonary fibrosis. A quantitative evaluation showed that the mean difference of left oblique, right horizontal and right oblique fissure to the reference was 2.06mm, 4.06mm and 2.85mm for healthy cases and 3.41mm, 5.79mm and 5.01mm for pathological cases.

## 1 Introduction

Human lungs are divided into five distinct anatomical regions, which are called the pulmonary lobes. The extraction of these lobes is of great importance in applications of lung disease assessment and treatment planning. For clinical applications, the distribution and location of pulmonary disease are beneficial for doctors to recognize pathogenesis, guide therapy and have further value in surgical planning. However, to find an effective and time-saving automatic lobe segmentation method is really challenging because of anatomical variation and incomplete fissures. On one hand, lobes vary between subjects. The anatomical variation of lobe is usually associated with age, sex and body type. Pathologies of diseased lungs usually deform the lobar shape abnormally and result in some fuzzy appearance of fissures on CT images. On the other hand, even in patients with healthy lung parenchyma the fissures are usually incomplete (Gülsün et al 2006).

In a broad sense, the existing computational lobar segmentation methods usually consist of two steps: the lung segmentation and the fissure detection. Currently, quite a number of lung segmentation methods are well established to get a reliable result. In contrast, most challenges for automated lobar segmentation lie in the fissure detection even though a number of researches have been involved in. One kind of fissure detection method makes use of either local or global knowledge of the anatomy of lung structure such as airway and vessel trees based on two features of lungs. The first feature is the fact that there should not be any large vessels in the vicinity of lobar fissures, so fissures should be located in the gaps between airway and vessel trees. Another feature is the vessels and bronchi could be classified into five lobe regions using an edge detection method. Another kind of method commonly makes use of gray-level information and shape information to detect the fissures. Generally, lobar fissures can be

regarded as bright planes crossing the pulmonary volume because of the higher density value of fissures comparing to the surrounding tissues. Based on this information, quite a number of published methods use local filtering algorithm to detect the voxels which lie on these planes, so that these detected voxel points can construct a continuous fissure surface. (van Rikxoot et al 2008, Ukil and Reinhardt 2009, Lassen et al 2013, Ross et al 2010, Doel et al 2012).

In this paper, we propose a statistical shape model (SSM) guided method to segment pulmonary lobes from CT images. We follow a three-step approach (Fig 1): in the first step, a thresholding based lung segmentation method is developed to get the lung boundary. In the second step, a statistical shape model is deformed to get a region of interest (ROI) of fissure locations. In the third step, the fissures are accurately located using the Hessian matrix combined with connected component filters and surface fitting algorithm. This method is able to detect fissures in all subjects, whereas existing segmentation tools failed in several subjects. Our new procedure does not depend on prior segmentation of anatomical structures (airway lobar classification) and has promising potential as a clinically useful automatic lobe segmentation procedure. A user-interactive interface is also developed for user to control and visualize the whole segmentation process and do some manual correction on the segmentation results.

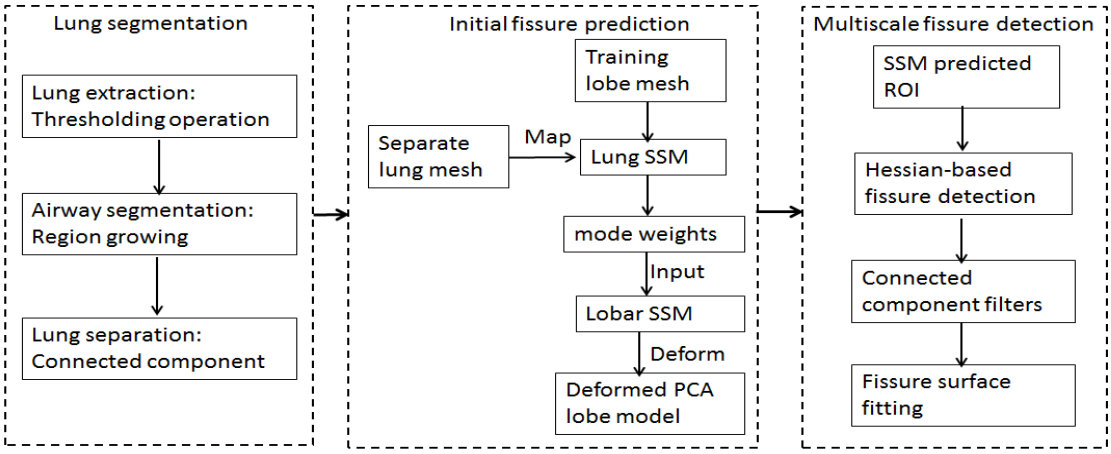


Fig. 1. Flow diagram of the lobar segmentation process.

## 2 Method

### 2.1 Lung segmentation

A good lung segmentation is a prerequisite for the next steps in this study, since all the other segmentations need perform inside the two lung regions. In this paper, we used a common thresholding method to segment lungs, the procedure is consist of the following steps: The method firstly uses a thresholding operation (-775 Hounsfield Units) and connected component identification to find the initial lung regions and trachea location. Use the highest point of trachea as a start point, a region growing technique is applied to detect the airway trees. Then, left and right lungs are separated as the two largest connected components remaining after removing the trachea and main left and right bronchi. Fig 2 shows the lung segmentation result.

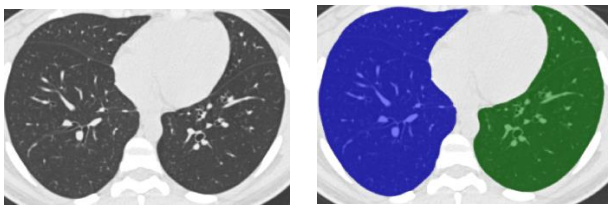

Fig. 2. Lung segmentation result. (a) Raw CT image. (b) Segmented lungs.

2.2 Initial fissure prediction

In the last twenty years, statistical shape model (SSM) based method has been widely used as one of the most successful methods for medical image segmentation. SSM makes use of statistical analysis to model shape variation, thus can be used to model and capture the shape difference and the mean shape among different people..

In this paper, A Statistical Finite element analysis of Lobe (SFeaL) which is based on the Active Shape Model (ASM) is constructed and deformed to predict the initial fissure locations for guiding the future accurate fissure detection. This approach employs finite element volume mesh to specify pulmonary lobar shape which provides an efficient parameterized representation of lobar boundaries and makes shape constraints available during image analysis. As any other statistical model guided segmentation, the first common step here is generating the statistical lobar mesh using a set of training data. To define lung shape, both left and right lung surface data cloud was created using the lung segmentation method introduced in section 2.1. The open-source visualization software CMGUI (https://www.cmiss.org/cmgui) was employed to manually digitize all three fissure points between adjacent lobes. A high-order (bi-cubic Hermite) finite element mesh template was then constructed for fitting the lung and fissure data cloud. By geometry-fitting the surface data to the mesh, we are able to mathematically describe a three-dimensional subject-specific lung shape. The left lung mesh has 35 nodes and 44 elements, while the right lung mesh has 50 nodes and 62 elements. Each node has 12 degrees of freedom (DoF) which store the global coordinates and first and second nodal derivatives. During the fitting process, a least square fitting optimization, which aimed to minimize the sum of the distances between each data point and its projection on to the nearest element was solved using CMISS (https://www.cmiss.org), a mathematical modeling environment. The average root mean square (RMS) error of this fitting method was 0.52mm averagely on the 30 training subjects (Fig 3(a)).

In the next stage, all the left and right nodes (85 nodes) were selected as pseudo landmarks to represent variations across the training cases. To remove the orientation and scaling differences between shapes, a General Procrustes Alignment (GPA) method was used to minimize the distance between two subjects through calculating the optimal rotation matrix and translation. The volumes of all the subjects were normalized to 1L during the processing (Fig 3(b)). The procrusted aligned meshes can be represented using the following expression:

$$\mathrm{B} = [\overline{x_1}\ \overline{y_1}\ \overline{z_1}\ \overline{x_2}\ \overline{y_2}\ \overline{z_2} \cdots \overline{x_p}\ \overline{y_p}\ \overline{z_p}]$$

Where p is the total node number of all the subjects (2550 nodes for our study, 30 subjects in total), and the over-line represents GPA to the mean. The matrix B was then decomposed into modes of variation by a Principal Component Analysis (PCA). Each mode symbolizes one type of lobe shape variation. PCA is a statistical procedure using an orthogonal transformation to help us find the principle components, which here are the modes with the most lobar shape variation through analyzing the eigenvectors and eigenvalues of the covariance matrix of the data matrix B. The results of principle components of variation showed that the first seven principal components account for over 90% of the total variation.

Now average statistical lobar shape model has been constructed with principal component nodes defined. To predict the fissure locations, a new volumetric CT subject is chosen which should be separated from the training subjects. The lung surface FE mesh without the fissure information is generated using the previous method and this lung surface mesh was then projected on to the

PCA-trained average lung statistical mesh (no fissure surfaces). The principal components' weight values were calculated from the projection and these weights were then used on the deformation of PCA-trained average lobar statistical mesh (with fissure surfaces) to derive an initial estimation of fissure locations (Fig 3(c) (d)).

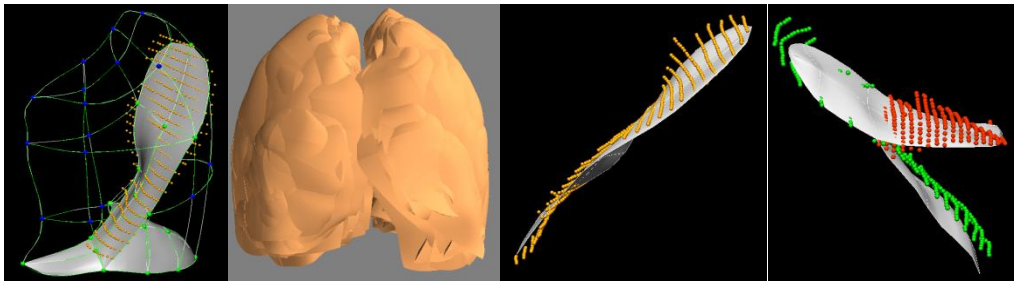

(a) (b) (c) (d)

Fig. 3. SSM based initial fissure prediction results. (a) Lung surface fitting and fissure digitizing manually. (b) Procrustes aligned meshes of 30 subjects. (c) (d) Fissure prediction compared to manual tracing points. White mesh is the predicted fissure surfaces.

2.3 Hessian-based multiscale fissure detection

In 3D space, fissures can be regarded as plane-like structure, since the grey-value increases rapidly from the structure border to the center and decrease again to the opposite border. Multiscale Hessian-based filters are thus used to enhance and differentiate these structures with specific shapes, i.e., blobs, sheets and tubes, which significantly describe the second order derivative information of imaging. The original CT image here was first applied by a Gaussian filter with a range of kernel sizes from 0.5mm to 2.5mm. Each kernel size gets a response and all the responses are then combined to get a maximum one for each voxel of the image. This multiscale operation guarantees a variety of sizes of fissures can be captured by Hessian. At each image voxel, the Hessian matrix was constructed as a symmetric matrix. Since for fissure structure, a light plane on a dark background is characterized by two large positive second derivatives across the plane and a small second derivative of either sign along the plane. Thus fissures modeled as plane should be reflected by a Hessian matrix having two small eigenvalues corresponding to the eigenvectors along the fissure planes and a large eigenvalue, since there is a strong curvature perpendicular to the fissure. So on the bright fissures, the relationship of eigenvalues $\lambda_1$, $\lambda_2$, $\lambda_3$ is defined as $|\lambda_1| \leq |\lambda_2| \leq |\lambda_3|$. $\lambda_1$ is expected to be large, while $\lambda_2$ and $\lambda_3$ are typically both low. From these characteristics, we can get a fissure probability of each voxel derived as follows:

$$\mathrm{S} = \tau S_{plane} S_{wall}$$

The first factor suppresses points whose largest eigenvalue $\lambda_3$is positive, since fissures are locally bright :

$$\tau = \begin{cases} 1, \lambda_3 < 0 \\ 0, \lambda_3 \geq 0 \end{cases}$$

Since the largest eigenvalue $|\lambda_3|$ should be much larger than the other two eigenvectors, the second factor detects plane or curve-like structures by searching for locations where $|\lambda_3|$ and $|\lambda_2|$ are significantly different. The third factor suppresses signals of noise such as blob-like structures, in contrast to plane-like fissures, have relatively large three eigenvalues. P and w are both set to 0.5 as thresholding in this study:

$$S_{plane} = \exp(-\frac{{S_{plane}}^2}{2p^2}), \quad R_{plane} = \frac{|\lambda_2|}{|\lambda_3|}$$

$$S_{wall} = \exp(-\frac{{R_{noise}}^2}{2w^2}), \quad R_{noise} = \sqrt{\lambda_1^2 + \lambda_2^2 + \lambda_3^2}$$

S gives a high response to the sheet local structures like fissures and suppresses all the other structures with low values. The result of an example of fissure enhancement filter can be seen in Fig 4(a).

Blood vessel points should be removed from the fissure enhanced result. The segmentation of vessels is achieved using a classical vessel segmentation method (Frangi et al 1998). It is also depend on a multiple scales (from 0.5mm to 3.0mm) Hessian-based enhanced filter, which similar to the fissure detection. The main difference is to detect the tube structure like vessels, the relationship of Hessian eigenvalues $\lambda_1$, $\lambda_2$, $\lambda_3$ should be defined as $|\lambda_1| \approx 0$, $|\lambda_1| \ll |\lambda_2|$, $|\lambda_2| \approx |\lambda_3|$. Fig 4(b) shows the result after eliminating the vessel voxels.

The initial fissure location predicted by average statistical shape model deformation gives us a region of interest (ROI) for an accurate fissure detection. The candidate points are selected within a certain distance of the initial fissure approximation, see Fig 4(c). It can help us remove most of the lung regions. Since there are still some spurious responses such as small plane-like structures on the result, a 2D 4-neighborhood connected component filter and a 3D 6-neighborhood vector-based connected component filter are employed successively to eliminate these noise. The vector-based connected component filter takes the largest eigenvector of Hessian matrix into consideration, as the largest eigenvector is perpendicular to the plane and it shows the orientation of fissure structure. The inner product of two adjacent normalized eigenvector is calculated as a criteria of component connection. Considering the fact that the curvature of a fissure is locally low, adjacent fissure voxels should have similar largest eigenvectors and large inner production. With applying the filters, all the small connected components whose volumes lower than a threshold are removed as noise from the 3D image, see Fig 4(d).

The detected points detected are then divided into a set of small subsections corresponding to different $(x', y')$. For each subsection, the point of the highest fissure probability (the highest S value) is selected as the finial candidate fissure point (Fig 4(e)). Then a continuous smooth fissure surface is generated using a B-spline method with a thin-plane spline and extrapolated to the lung boundaries, see Fig 4(f).

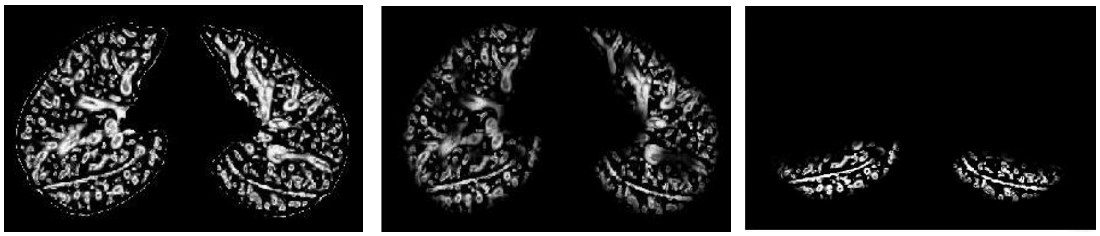

(a) (b) (c)

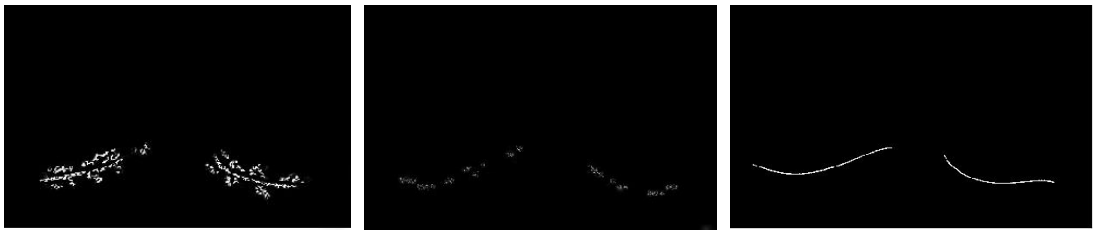

(d) (e) (f)

Fig.4. Hessian-based multiscale fissure detection results. (a) Hessian-based fissure enhancement. (b) Remove vessel voxels. (c) ROI of fissure locations based on SSM projection. (d) 2D and 3D eigenvector based connected component filter. (e) Fissure candidate points. (f) B-spline curve fissure surface fitting.

2.4 Interactive user control interface

As we discussed above, a series of parameter values need to be chosen correctly to ensure a successful lobar segmentation. However, one fixed value of parameter is usually not suitable for all the subjects due to a wide variation of lung tissue and fissure appearances across the population. Therefore, a fast and convenient interactive way to control the segmentation procedure is reasonable and acceptable. Based on an open source Pulmonary Toolkit (PTK, https://github.com/tomdoel/pulmonarytoolkit), we developed an improved user-friendly interactive interface to control the segmentation parameters as input. By making use of some built-in objects and visualization system of PTK, we add our lobar segmentation algorithm into the algorithm package and make parameter control buttons available on the interface (Fig 5).

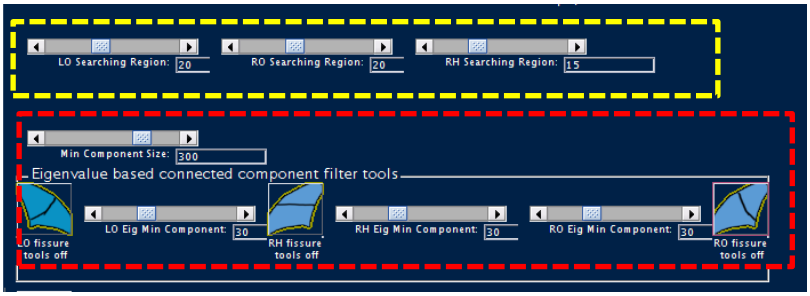


Fig. 5. User interactive interface. The yellow frame shows the slides for changing search region size of fissure detection, the red frame shows the slides for changing connected component sizes for each filter.

## 3 Experiment

3.1 Data

We tested our automatic lobar segmentation method on two different kinds of datasets : 1) CT images of young normal volunteers taken at different lung volumes and with different thickness. These normal subjects are selected from Human Lung Atlas (HLA) dataset which is approved by the University of Iowa Institutional Review Board and Radiation Safety Committees. The selected subjects are consists of 5 functional residual capacity (FRC) cases and 5 total lung capacity (TLC) cases. Slice thickness was 0.5-0.7mm. 2) Clinical CT images of old patients diagnosed with idiopathic pulmonary fibrosis (IPF) disease. These diseased subjects are acquired from Auckland District Health Board (ADHB) under the supervision of Dr. Wilsher, following ethics committee approval for this study. Slice thickness was 1.25-3mm.

3.1 Result

To assess the accuracy of the automatic lobar segmentation method in the normal and disease subjects, we compared the automatic segmentation results to the manual ones with digitized all the three fissures. The fissure points were clicked on 2D cross sections and sagittal slices manually. The quantitative evaluation of the segmentation accuracy was assessed from computing the mean difference and the percentile measurement. The mean difference is defined as the mean distance between each manual fissure point and its closet voxel in automatic lobar

segmentations:

$$d_i^{min} = \min_j \left\{ \sqrt{(x_j^a - x_i^m)^2 + (y_j^a - y_i^m)^2} \right\}$$

$$d_{mean} = \frac{(\sum_{i=1}^{n} d_i^{min})}{n}$$

Where $(x_i^m, x_i^m)$ is the manually-defined contour voxel location and $(x_i^a, x_i^a)$ is a computer-defined contour voxel location. The quantitative analysis of the segmentation result is shown in Fig 6.

The percentile measurement is defined as the percentage of the distance between manual and automatic point under 3mm criteria, following the equation:

$$\sqrt{(x_i^a - x_i^m)^2 + (y_i^a - y_i^m)^2} \leq 3\text{mm}$$

since 3mm approximates the thickness of clinical CT images that surgeons and radiologists read in clinical settings.

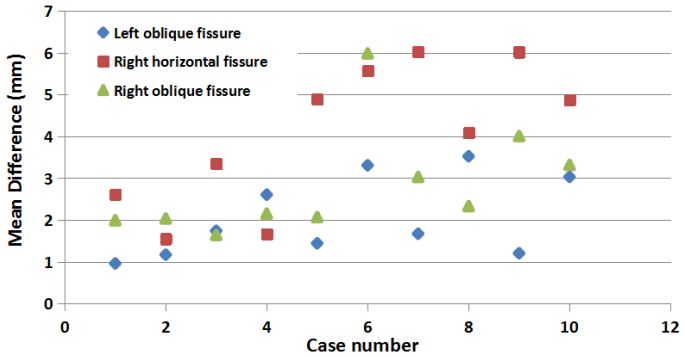


(a)

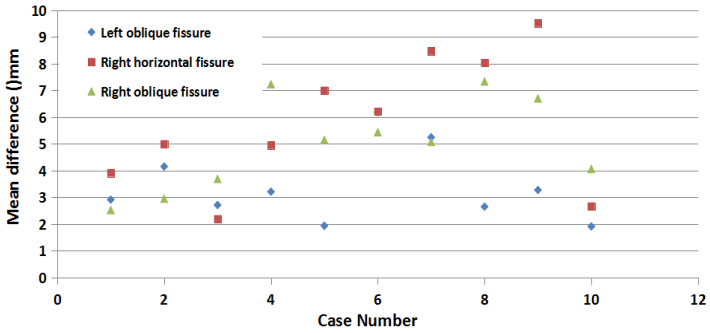


(b)

Fig.6. Quantitative evaluation results of the segmentation accuracy. (a) Mean difference of normal young subjects. (b) Mean difference of IPF old subjects.

The average mean difference assessed on normal subjects and IPF subjects are 2.06mm, 4.06mm, 2.85mm and 3.41mm, 5.79mm, 5.01mm for left oblique, right horizontal and right oblique fissure respectively. The average percentile accuracy on normal subjects and IPF subjects are 78.39%, 61.62%, 72% and 65.86%, 55.94%, 60.06% for left oblique, right horizontal and right oblique fissure respectively. Due to the lower resolution and pathologic abnormalities, IPF subjects got a worse accuracy. In addition, the segmentation method performs well on left oblique fissure than right oblique fissure and right horizontal fissure, because left lung has simpler anatomic structure with only one fissure, in contrast, misdetection happens more often in the area of right lung

where the two fissures are closed. See Fig 7, which shows the accuracy distribution of the three fissures with different colors. It can be seen that the method causes higher error in the lung boundary area, since the fissures here are commonly incomplete, thus few fissure candidate points can be detected accurately.

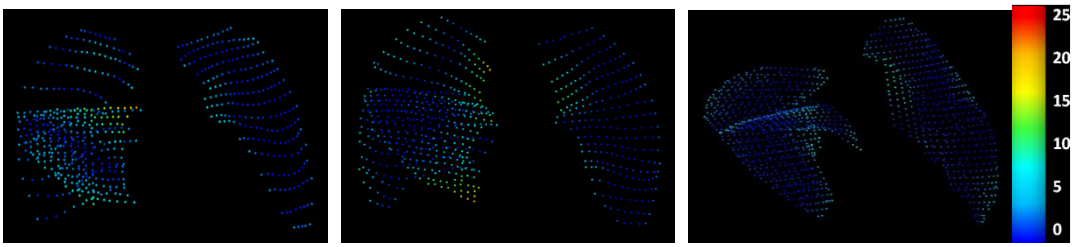


(a) (b) (c)

Fig.7. Accuracy distribution results of some example subjects.

In addition, current published studies show that it seems impossible to ensure one fully automatic lobar segmentation method perform perfectly on all kinds of subjects, especially for some diseased abnormal cases. Therefore, we developed a correction tool on the user interface to improve the result manually, as shown in Fig 8.

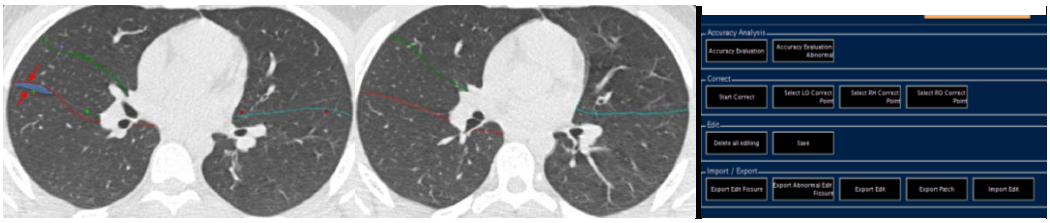

(a) (b) (c)

Fig. 8. Fissure manual correction procedure. (a) Fissures before correction, the blue region is the corrected region. (b) Fissures after correction. (c) The interface for operating correction.

## 4 Conclusions and Discussions

In this paper, we present an automatic pulmonary lobar segmentation method combined with some manual interaction. The result shows that our segmentation method can perform well on CT images of normal subjects and get a relative accurate result for most of the IPF abnormal subjects. In the future work, a statistical shape model dataset could be developed. The dataset could contain different kinds of statistical model for different ages, sexes, lung volume or diseases, since it can help us prediction a more accurate ROI for the future fissure detection. Meanwhile, the method need to be assessed on more diseased subjects and be improved combined with the disease characteristic of these images. A user-friendly interaction and more time-saving programming is also a key point in the future study.

## Reference